Dent Imperfections in Shell Buckling: The Role of Geometry, Residual Stress, and Plasticity

S. Gerasimidis[1]
Department of Civil and Environmental Engineering,
University of Massachusetts,
Amherst, MA 01003
e-mail: sgerasimidis@umass.edu

J. W. Hutchinson
School of Engineering and Applied Sciences,
Harvard University,
Cambridge, MA 02138
e-mail: jhutchin@fas.harvard.edu

Departures of the geometry of the middle surface of a thin shell from the perfect shape have long been regarded as the most deleterious imperfections responsible for reducing a shell's buckling capacity. Here, systematic simulations are conducted for both spherical and cylindrical metal shells whereby, in the first step, dimple-shaped dents are created by indenting a perfect shell into the plastic range. Then, in the second step, buckling of the dented shell is analyzed, under external pressure for the spherical shells and in axial compression for the cylindrical shells. Three distinct buckling analyses are carried out: (1) elastic buckling accounting only for the geometry of the dent, (2) elastic buckling accounting for both dent geometry and residual stresses, and (3) a full elastic–plastic buckling analysis accounting for both the dent geometry and residual stresses. The analyses reveal the relative importance of the geometry and the residual stress associated with the dent, and they also provide a clear indicator of whether plasticity is important in establishing the buckling load of the dented shells. [DOI: 10.1115/1.4048807]

Keywords: buckling, cylindrical shells, spherical shells, imperfections, residual stress, plasticity

1 Introduction

Major efforts are underway to revise design codes for shell buckling [1,2] which will place more emphasis on the analysis and quality assessment of the shell with the intent of allowing designs that are less conservative than those permitted by current design criteria based heavily on shell buckling experiments. It has been a long-held view that the most deleterious imperfections for unstiffened shell structures are geometric departures of the middle surface from the perfect shape, assuming support conditions are adequate. This view almost certainly arose after the pioneering work of von Kármán and Tsien [3], Koiter [4], and others showed that relatively small geometric imperfections could explain the significant reductions below the predictions for perfect shells of experimentally measured buckling loads. However, it is not known to what extent factors other than imperfection geometry contribute to the buckling loads seen in the large experimental data sets for cylindrical and spherical metal shells [5,6] used to establish design knockdown factors. In this paper, we carry out a systematic study to parse the roles of geometric imperfection, residual stress, and plasticity in contributing to the buckling load reductions of metal spherical and cylindrical shells. Our focus is primarily on shells designed to buckle elastically, although the role of material yield stress will be exposed. Specifically, we carry out a two-step analytical process whereby the shell is first indented into the plastic range to create a localized dent with the accompanying residual stresses. Then, in the second step, the shell is analyzed to ascertain the buckling reduction caused by the dent imperfection. In the second step, we carry out both elastic and elastic–plastic buckling analyses and, to see the effect of the residual stress, we carry out the analyses both with and without the residual stress.

While we are unaware of studies similar to the one to be presented in this paper which focus on residual stresses accompanying localized dimple-like imperfections, there is a substantial literature on the influence of residual stress on buckling of welded shell structures, e.g., Refs. [7–9], dealing with both thick and thin walled shells. There is also a small literature on the residual stresses in cylindrical shells formed by plastically bending flat plates into cylinders by various means, e.g., Refs. [10,11]. Most of these studies have been concerned with relatively thick-walled shells which buckle in the plastic range.

Recent analytical and computational research on the imperfection-sensitivity of elastic shell buckling has placed emphasis on localized dimple-like imperfections which are generally regarded to be more realistic than imperfections in the shape of the buckling modes which generally extend in a highly correlated manner over the entire shell [12–14]. The present study follows in this path by focusing on dimple, or dent, imperfections created by indenting the shell into the plastic range. Sections 2 and 3 deal with spherical shells, and Secs. 4 and 5 deal with cylindrical shells. The first two sections on each type of shell presents results on the creation of the dent, while the second of the two sections gives results from several buckling analyses used to parse the roles of the geometric imperfection, residual stress, and plasticity. The nonlinearity and buckling behavior of the spherical shell is such that the analysis can be meaningfully confined to axisymmetric behavior within a framework of ordinary differential equations, allowing for consideration of all the important parameters. For the cylindrical shell, the essential nonlinear buckling behavior is inherently two-dimensional, and a commercial code has been employed to perform both steps of the analyses.

2 Spherical Shells: Step 1, Creating the Dent Imperfection

The first step in the set of simulations is the indentation of the perfect spherical shell to create the imperfection. Equal and opposite inward-point forces are applied at the shell's poles with magnitude large enough to cause plasticity. Then, upon reducing the forces to zero, an axisymmetric dimple-shaped dent remains at each pole accompanied by an axisymmetric residual stress distribution. The shell has radius R and thickness t. The shell is elastically isotropic with Young's modulus E and Poisson's ratio ν. Reference

[1]Corresponding author.

Contributed by the Applied Mechanics Division of ASME for publication in the Journal of Applied Mechanics. Manuscript received September 10, 2020; final manuscript received October 9, 2020; published online December 4, 2020. Assoc. Editor: Annie Ruimi.

throughout this section and the next will be to the elastic buckling pressure of the perfect shell, p_C, and the associated compressive equi-biaxial membrane stress at buckling

$$p_C = \frac{2Et^2}{\sqrt{3(1-\nu^2)}R^2}, \quad \sigma_C = \frac{Et}{\sqrt{3(1-\nu^2)}R} \tag{1}$$

The plastic behavior of the shell is also taken to be isotropic and characterized by J_2 flow theory. The tensile (and compressive) yield stress is σ_Y, the hardening exponent is N, and the tensile stress–strain curve (with continuous slope at yield) is

$$\varepsilon = \frac{\sigma}{E}, \quad \sigma \le \sigma_Y; \quad \varepsilon = \frac{\sigma_Y}{E}\left(\frac{\sigma}{\sigma_Y}\right)^{1/N} + \frac{1}{E}\left(1-\frac{1}{N}\right)(\sigma-\sigma_Y), \quad \sigma > \sigma_Y \tag{2}$$

with σ as stress and ε as strain.

The strain–displacement relations of shell theory used for the axisymmetric deformations of the spherical shell are those of the small strain-moderate rotation theory of Sanders [15] and Koiter [16]. All the calculations in this paper assume the behavior of the spherical shell is symmetric about the equator with θ as the meridional angle measured from the equator. The problems considered are described by a sixth-order nonlinear system of first-order ordinary differential equations (ODEs) employing the vector of unknowns (Q, M_θ, N_θ, φ, w, u) where, in standard shell theory notation, Q is the transverse shear force/length, M_θ is the meridional resultant moment, N_θ is the resultant meridional in-plane stress, φ is the rotation, w is the outward normal displacement, and u is the tangential displacement. The formulation of the incremental equations and the solution method is outlined in Ref. [17]. A finite difference method is employed for numerical solution and most of the simulations used 200 equally spaced nodal points between equator and pole. Each incremental load step requires incremental moduli averaged through the thickness relevant to the shell theory formulation to be computed using the plasticity formulation. For this purpose, stresses in the shell are saved at 8 points through the thickness at all the midpoints between the equally spaced nodes.

An inward force of magnitude P directed toward the center of the sphere is applied at the pole to indent the shell, first increased to a maximum value and then unloaded back to zero. Symmetry boundary conditions consistent with no external constraint are applied at the equator. This process is illustrated in Fig. 1(*a*) for three values of the maximum force labeled as A, B, and C. This example is computed for a shell with $R/t = 200$, $\nu = 0.3$, $\sigma_Y/\sigma_C = 1$, and $N = 0.25$. The nonlinearity of the monotonically increasing curve of force versus inward pole deflection is due to both the nonlinear elastic behavior of the shell and plasticity, with plasticity first occurring in this example for $PR/2\pi D \cong 1.5$ and $-w_{pole}/t \cong 0.5$. The elastic bending stiffness is $D = Et^3/12(1-\nu^2)$. The residual dent shape after unloading for each of the three maximum indentation forces is plotted in Fig. 1(*b*) with $w(\theta)$ as the outward normal displacement of the shell middle surface. For a shell with $R/t = 200$, the center of the dent to its edge extends roughly 10 deg. The width of the residual dent increases with increasing denting force and resulting dent amplitude. Figure 1(*c*) plots the distribution for case C of the three residual shell stress quantities. These are the stress quantities (in addition to the dent shape) that enter the elastic buckling calculations in Step 2 in Sec. 3 which account for the residual stresses in the shell.

To deal with the singularity at the pole due to the concentrated indentation force, we have taken a very small section of the shell at the pole within the region $\beta \le \beta_0$ to be rigid, with angle $\beta = \pi/2 - \theta$ measured from the pole and

$$\beta_0 = 0.048\left(\sqrt{1-\nu^2}R/t\right)^{-1/2} \tag{3}$$

For a shell with $R/t = 200$, $\beta_0 = 0.2$ deg; the small influence of this modification is discussed and illustrated in Ref. [18]. When the yield stress is scaled such that σ_Y/σ_C remains fixed, the dimensionless curves of $PR/2\pi D$ versus $-w_{pole}/t$ in Fig. 1(*a*) are independent of R/t for thin shells (e.g., R/t larger than about 25). For reference, $\sigma_Y/\sigma_C = 1$ implies that $\sigma_Y/E = 0.00303$ if $R/t = 200$. The shapes of the dent in Fig. 1(*b*) are also independent of R/t if they are plotted using the polar angle scaled as $\beta\left(\sqrt{1-\nu^2}R/t\right)^{1/2}$.

With δ denoting the inward deflection of the shell middle surface of the residual dent at the pole, i.e., $\delta = -(w_{pole})_{\text{res}}$, the normalized dent amplitude for three values of σ_Y/σ_C is plotted as a function of the maximum imposed pole deflection during indentation in Fig. 2(*a*) and as a function of the maximum imposed indentation force in Fig. 2(*b*). The amplitude range of δ/t plotted in Fig. 2 is the relevant range for the present study. Figure 2(*c*) is a plot of the residual meridional in-plane resultant stress, $\bar{N}_\theta$, averaged over the circular region at the pole of radius $2.5\sqrt{Rt}$ (approximately 10 deg for $R/t = 200$) and normalized by $\sigma_Y t$. One sees from this plot that the ratio of residual compressive stress associated with the dent to the yield stress depends almost entirely on the dent amplitude δ/t with little dependence on σ_Y/σ_C in the range of interest in this paper. This finding will be seen to have implications for buckling. We have re-computed these curves using a strain hardening index $N = 0.1$ rather than $N = 0.25$. The two sets of curves are similar with no difference of any significance for our purposes. As for the case in Figs. 1(*a*) and 1(*b*), the dimensionless plots in Fig. 2 are found by

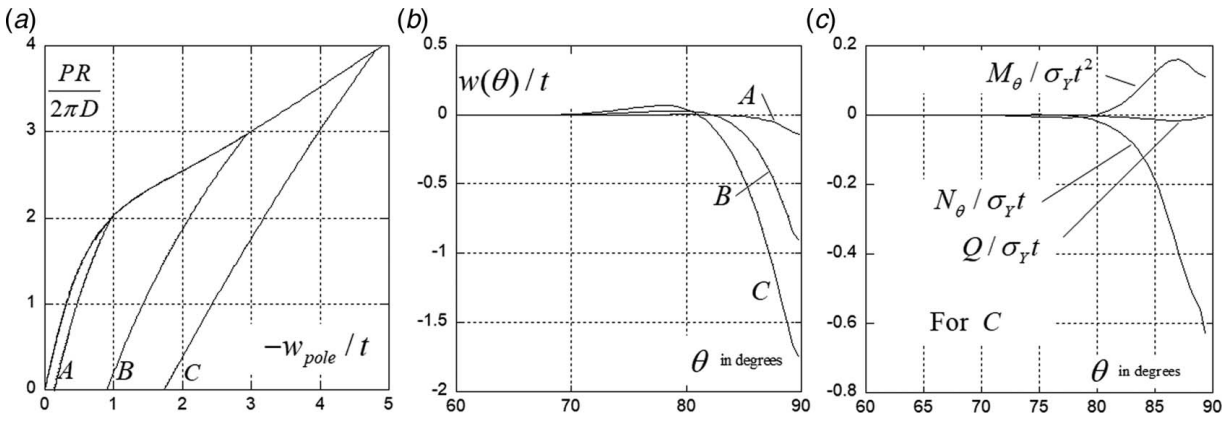

Fig. 1 Illustration of the creation of a dent imperfection in Step 1. (*a*) Dimensionless inward directed pole force versus inward pole displacement normalized by shell thickness, including unloading back to zero pole force, for maximum forces of $PR/2\pi D = 2$, 3, and 4. (*b*) Residual dent shape for the three maximum forces. (*c*) Distribution of the normalized residual values of Q, M_θ, and N_θ for the maximum force corresponding to C. These were computed for $R/t = 200$, $\nu = 0.3$, $\sigma_Y/\sigma_C = 1$, and $N = 0.25$.

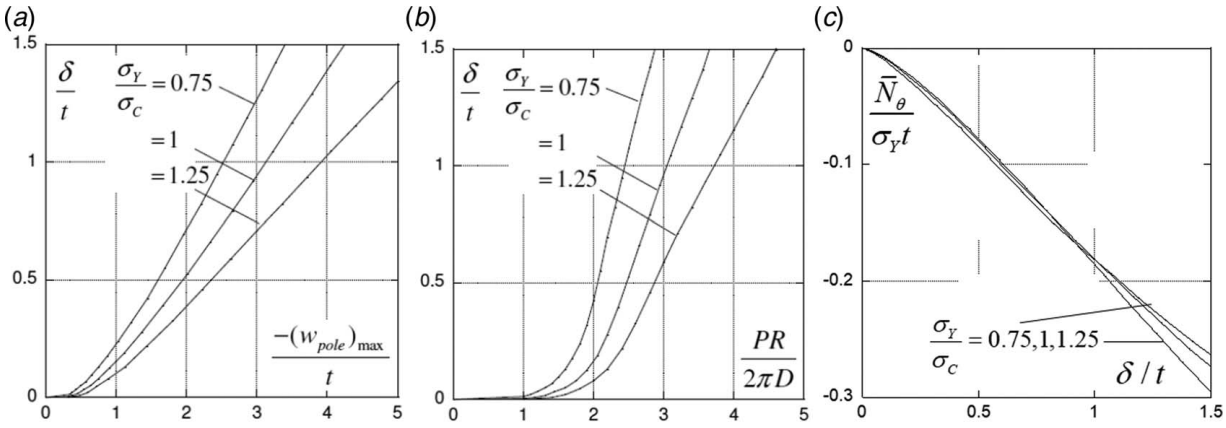

Fig. 2 Residual dent amplitude normalized by shell thickness, δ/t, (*a*) versus maximum inward indentation pole deflection and (*b*) versus maximum indentation force for three values of σ_Y/σ_C for a shell with $R/t=200$, $\nu=0.3$, and $N=0.25$. (c) The resultant stress component, N_θ, normalized by $\sigma_Y t$ and averaged over the circular region at the pole of radius $2.5\sqrt{Rt}$ for the same three ratios of σ_Y/σ_C. The curves are essentially independent of R/t with these dimensionless variables.

performing calculations with different R/t to be essentially independent of R/t if $R/t>25$.

3 Spherical Shells: Step 2, Buckling of the Dented Shell Under External Pressure—Three Analyses

To set the stage for this section, we begin by presenting results for the buckling of a spherical shell with a "standard" geometric dimple imperfection [14] that is subject to external pressure. Both elastic and elastic–plastic buckling calculations are performed which reveal important insights into the role of the dimensionless yield stress parameter, σ_Y/σ_C, in the buckling of imperfection-sensitive shells. Identical axisymmetric geometric dimple imperfections (with no residual stresses) are introduced at each pole having an initial normal deflection of the middle surface given by (at the north pole)

$$w_I(\beta)=-\delta e^{-(\beta/\beta_I)^2} \text{ with } \beta_I=B\left(\sqrt{1-\nu^2}R/t\right)^{-1/2} \tag{4}$$

The buckling pressure for a given imperfection amplitude δ is the maximum pressure the shell can support. The buckling pressures in Fig. 3 have been computed for 30 values of δ/t over the range shown. The elastic buckling pressure, computed with an elastic version of the code, lies just above the elastic–plastic computation for $\sigma_Y/\sigma_C=1$, and an elastic–plastic calculation with $\sigma_Y/\sigma_C=1.25$ (not plotted in Fig. 3) is identical to the elastic result, implying that up to the maximum pressure, no plastic yielding occurs for any of the imperfect shells. For lower yield stresses, e.g., $\sigma_Y/\sigma_C=0.75$ and 0.5, plastic deformation does occur before the shell reaches the maximum support pressure and this results in a lower buckling pressure, more so for smaller imperfection amplitudes than for larger amplitudes.

The dimensionless plots in Fig. 3 reveal an important feature of spherical shell buckling [19] which has also been observed for cylindrical shells under axial compression [20]. With geometric imperfections, the maximum pressure (or maximum axial load for the cylinder) is attained while the shell is still in the elastic range if $\sigma_Y/\sigma_C\geq 1$, or at worse the shell only experiences minimal

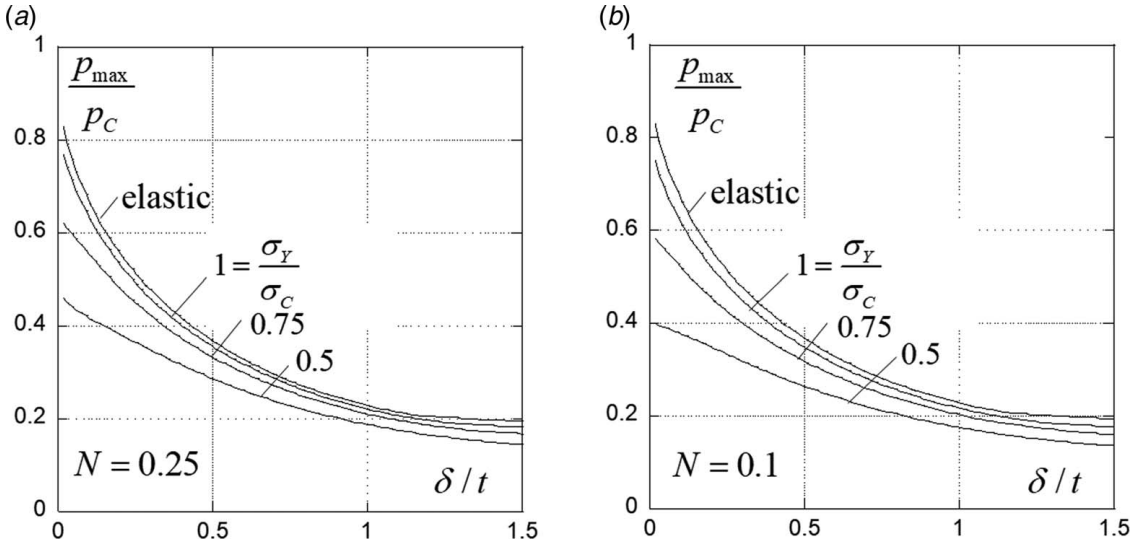

Fig. 3 Buckling pressure as dependent on the amplitude of a geometric dimple imperfection (4) with no residual stresses for a strain hardening exponent (*a*) $N=0.25$ and (*b*) $N=0.1$. The top curve is based on an elastic calculation, while the other three curves are based on an elastic–plastic calculation. With $\sigma_Y/\sigma_C=1.25$, the elastic–plastic calculation is identical to the elastic prediction implying no plasticity occurs prior to the maximum pressure. These curves have been computed with $R/t=200$, $\nu=0.3$, and $B=1.5$, but they are independent of R/t.

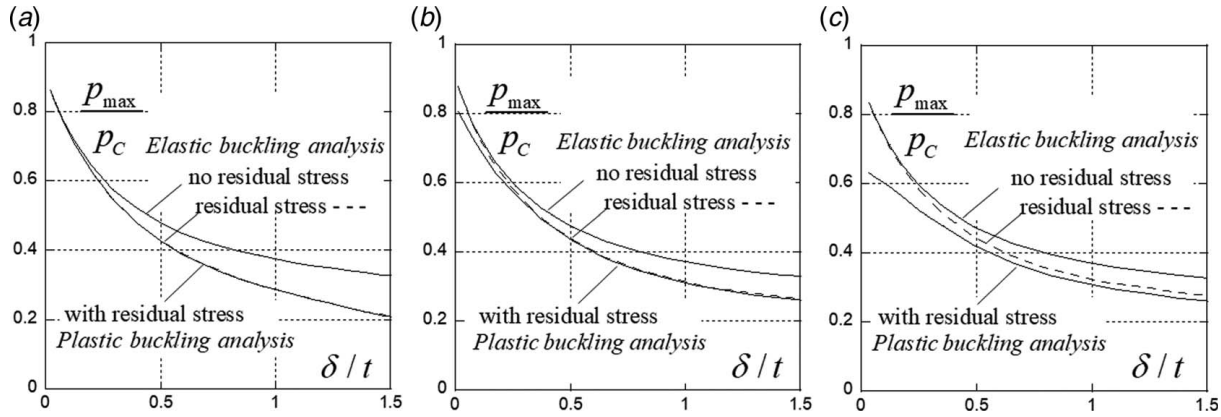

Fig. 4 Buckling of the dented spherical shell subject to external pressure for (*a*) $\sigma_Y/\sigma_C = 1.5$, (*b*) $\sigma_Y/\sigma_C = 1$, and (c) $\sigma_Y/\sigma_C = 0.75$. Results of three types of buckling analyses are plotted: an elastic analysis accounting only for the geometry of the dent, an elastic analysis accounting for both the dent geometry of the dent and residual stresses, and an elastic–plastic analysis accounting for the dent geometry and residual stresses. The calculations have been made with $R/t = 200$, $\nu = 0.3$, and $N = 0.25$, but the curves are independent of R/t.

plastic yielding. The primary focus in this paper will be on shells that have been designed to buckle elastically, and thus, we will be mainly interested in shells whose yield stress is no less than the buckling stress of the perfect shell, i.e., $\sigma_Y/\sigma_C \geq 1$. However, to provide additional insight, we will show some results for $\sigma_Y/\sigma_C = 0.75$. The study of cylindrical shells under axial compression in Secs. 4 and 5 feature the geometry and material properties representative of a typical aluminum soda can with $\sigma_Y/\sigma_C = 1.95$. One should be aware that the dramatic reduction of the load at buckling as a function of the imperfection amplitude characterizing spheres under external pressure and cylinders under axial compression helps explain why plasticity does not occur before the onset of buckling in the imperfect shells if $\sigma_Y/\sigma_C \geq 1$. The same may not necessarily be true for modestly imperfection-sensitive shell structures such as the cylindrical shell under external pressure or for columns and flat plates under compression, as discussed again in Sec. 6.

Now, we consider buckling under external pressure of the spherical shells dented in Step 1. As mentioned in Sec. 1, three types of buckling analyses will be used in Step 2 to parse the relative importance of imperfection geometry, residual stress, and the influence of any additional plasticity prior to buckling. For each dented shell, two elastic buckling calculations will be made, one accounting only for the geometry of the dent and the other including both the geometry and residual stresses. The third calculation for each dented shell is an elastic–plastic analysis, accounting for dent geometry and residual stresses, whose purpose will be to determine if plasticity occurs prior to buckling during application of the pressure and, if so, what effect it has on the buckling pressure. In the elastic–plastic buckling analysis, the full details of the plasticity distribution through the shell at the nodal midpoints are used; for each dent amplitude, the buckling analysis in Step 2 follows Step 1 seamlessly as a second form of loading.

To recapitulate, a perfect spherical shell with prescribed parameters (R/t, ν, σ_Y/σ_C, and N) is first dented (Step 1), and then, this same shell, which is otherwise unloaded, is subject to external pressure (Step 2). The maximum pressure the shell can support is identified as the buckling pressure and computed by each of the three methods mentioned earlier. The plots in Fig. 4 summarize results for three levels of yield stress. For each of the three yield stresses in Fig. 4, 25 shells indented over a range of dent amplitudes up to $\delta/t = 1.5$ were subsequently analyzed for buckling by the three methods. The shells in Fig. 4 have $R/t = 200$, but the curves in this figure are essentially independent of R/t. The curves have also been computed for a hardening exponent $N = 0.1$ and do not differ significantly from those plotted.

Begin by considering the shells in Figs. 4(*a*) and 4(*b*) which we have previously designated as having been "designed to buckle elastically." The first thing to note is that this designation is indeed justified. The elastic analysis which includes residual stress and the complete elastic–plastic analysis which includes the entire prior residual history are identical for $\sigma_Y/\sigma_C = 1.5$ and virtually identical for $\sigma_Y/\sigma_C = 1$, except for very small dent amplitudes where plasticity does slightly reduce the buckling pressure. Moreover, by comparing the two analyses which account for residual stresses with the elastic analysis that accounts only for dent geometry (the upper curve in each plot), one immediately sees that geometry accounts for a large fraction of the buckling pressure reduction for these imperfections. This confirms the long, widely held notion that imperfection geometry is the dominant contributor to imperfection-sensitivity. However, this conclusion must be tempered by the fact that accounting for the residual stress does lower the buckling pressure in these examples by an amount that should not be ignored, particularly so for the larger dent amplitudes. Furthermore, note that the effect of the residual stress is larger for the shells in Fig. 4(*a*) with the higher yield stress. This is easy to understand: For a given dent amplitude, the higher the yield stress of the material, the higher the stress need to create the dent and thus the higher the residual stress. This trend is consistent with the results in Fig. 2(*c*) that indicate that the residual in-plane stress for a given dent amplitude is proportional to the yield stress with little influence from σ_Y/σ_C.

The main insight to emerge from the results in Fig. 4(*c*) for the shell that is not designed to buckle in the elastic range (having $\sigma_Y/\sigma_C = 0.75$) is that plasticity occurring during the pressure loading does indeed lower the buckling pressure below what both elastic analyses predict. This effect of plasticity is largest for the smaller dent amplitudes, not surprisingly because the perfect undented shell will buckle almost immediately after the membrane stress reaches yield, that is, when $p \cong 0.75 p_C$. It should be mentioned that no attempt has been made in this paper to analyze the plastic bifurcation problem for the perfect shell when $\sigma_Y/\sigma_C < 1$. It is well known that the J_2 flow theory of plasticity employed in this study tends to be overly stiff leading to bifurcation predictions for perfect shells (and plates) that often exceed those obtained using theories with yield surfaces having higher curvature or corners, and often higher than experimental findings. Nevertheless, once the imperfection amplitude becomes non-negligible, the dependence of buckling predictions on yield surface curvature tends to disappear, as illustrated for spherical shells in Ref. [17]. We do not believe the choice of plasticity theory has an appreciable influence on the results in Figs. 2 through 4 nor those for cylindrical shells to follow.

Finally, it is also worth remarking that a dent imperfection with an amplitude δ/t is not quite as deleterious to buckling as the "standard" dimple imperfection as can be seen by comparing the results in Fig. 4 with those in Fig. 3.

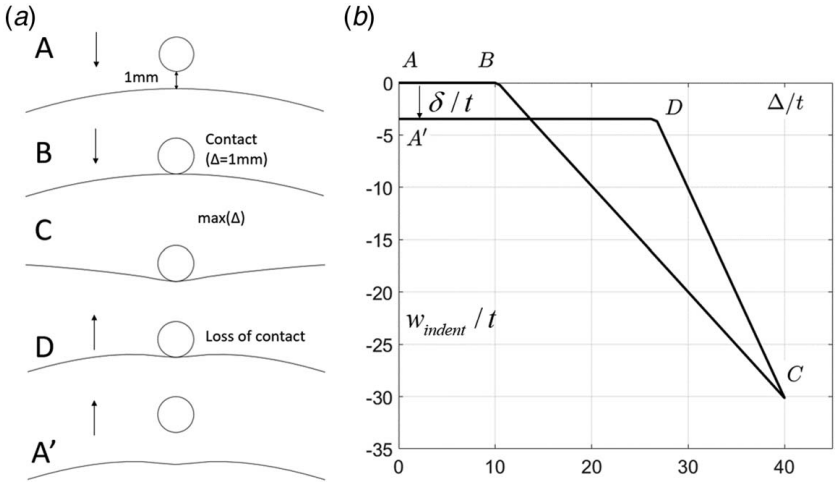

Fig. 5 Creating the dimple dent in the cylindrical shell. (*a*) The loading and unloading indentation process. The associated history of (*b*) shell displacement, w_{indent}, under the indenter versus imposed displacement of the indenter, Δ. The residual dent amplitude is δ.

4 Cylindrical Shells: Step 1, Creating the Dent Imperfection

The indentation process creating a dent for the cylindrical shell is essentially the same as that for the spherical shell. For the cylindrical shell, however, the process is not axisymmetric and the commercial finite element code, ABAQUS STANDARD [21], has been used to carry out the calculations. A specific shell is used to illustrate the indentation process and the subsequent buckling calculations in Step 2: it is a clamped cylindrical shell with dimensions and material properties of a typical aluminum soda can that has been tested extensively and analyzed [22]. The shell's length, radius, and thickness are $L = 104.1$ mm, $R = 28.6$ mm, and $t = 0.1$ mm such that $L/R = 3.64$ and $R/t = 286$. The plasticity theory employed is again J_2 flow theory with the stress–strain curve (2) using $E = 69$ GPa, $\nu = 0.3$, $\sigma_Y = 285$ MPa, and $N = 0.1$. The cylindrical shell with these dimensions and material properties will be referred to as the "reference shell." The classical buckling load (axial force) and associated compressive axial stress for a perfect elastic cylindrical shell are

$$F_C = \frac{2\pi Et^2}{\sqrt{3(1-\nu^2)}}, \quad \sigma_C = \frac{Et}{\sqrt{3(1-\nu^2)}R} \tag{5}$$

The classical buckling stress for the shell dimensions listed above is $\sigma_C = 146$ MPa, and thus, the reference shell has $\sigma_C/\sigma_Y = 1.95$. In the terminology of this paper, the reference shell used to illustrate the effect of dent imperfections has been designed to buckle elastically. The effect of decreasing the yield stress for this shell will also be investigated.

The computational details follow those presented in Ref. [13] where the effect of geometric dimple imperfections has been studied. Step 1 indents a perfect shell, and Step 2 buckles the dented shell under axial compression. The mesh for the models was created by user-written codes; S4R elements with an element length of 0.914 mm in both axial and circumferential directions, which is roughly $0.5\sqrt{Rt}$. For the integrations, 11 section points through the thickness of the shell were selected. At the two ends of the cylindrical shell, two nodes (one at each end) were defined at the center of the circular cross section. These central nodes were used to apply the boundary conditions at each end of the shell. The central node at each end of the shell is connected with rigid links to the other nodes at the end of the shell. The rigid links constrain both the translational and rotational degrees-of-freedom with respect to the central node. Using this procedure, the simulations enforce clamped boundary conditions at both ends and prescribed end-shortening Δ.

Overall rotation of the ends is suppressed. The geometrically nonlinear Riks arc length analysis was used to follow the nonlinear solutions. The indentation of the shell is performed using a rigid spherical indenter (results for 3 indenter radii will be presented, $R_I = 1$, 1.5, and 2.5 mm). At the start of the indentation process, the nearest point on the indenter is located 1 mm away from the shell mid-surface. A displacement of the sphere is imposed which translates it toward the shell. Contact between the rigid sphere and the shell is assumed to be a hard contact, and the option for separation during unloading is enabled. The tangential behavior of the contact interaction between the sphere and shell is assumed to be frictionless.

The loading and unloading process used to create the dent in the reference cylindrical shell is illustrated in Fig. 5 for an indenter with $R_I = 1$ mm. The center of the dent is located at a point along the mid-length circumference. In the example shown, the indenter is displaced a maximum of 40 times the shell thickness to C (30 times the shell thickness after first contact) and then retracted back to its original position, A'. Plastic deformation occurs during

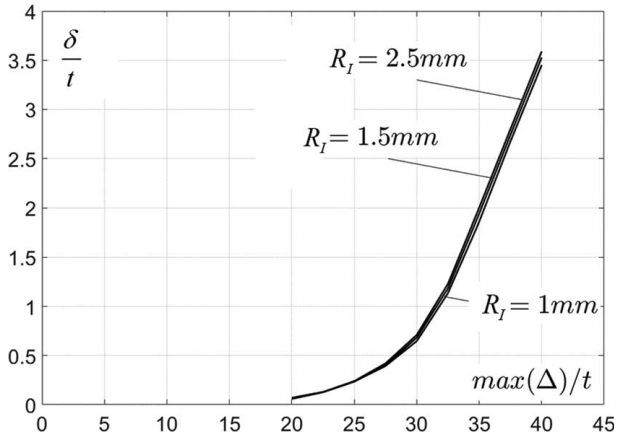

Fig. 6 Amplitude of the residual dent normalized by the shell thickness as a function of the maximum imposed indenter displacement normalized by the thickness. These results have been computed for the reference shell cited in the text with three different radii of the indenter.

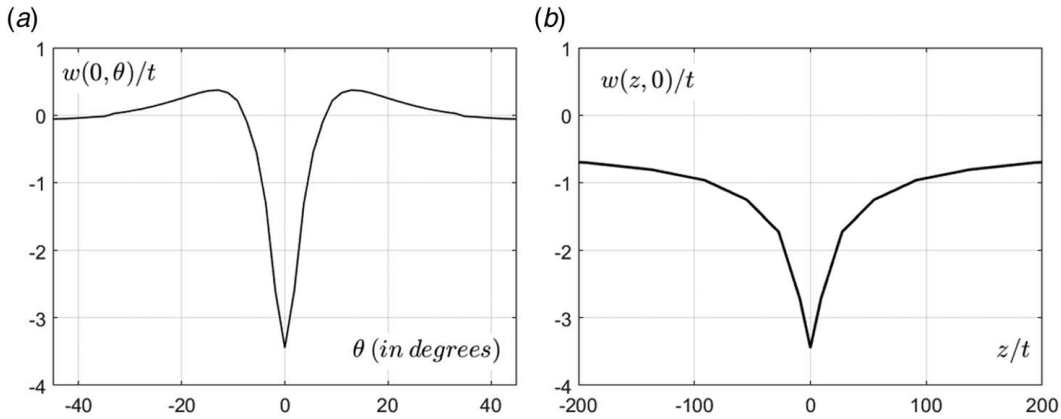

Fig. 7 The shape of the residual dent in the reference cylindrical shell as created by the indenter with R_I = 1 mm and max(Δ)/t = 40: (*a*) along the circumferential arc passing through the center of the dent and (*b*) along the axial line passing through the center of the dent. The coordinates (θ, z) are the circumferential angle and axial distance both measured from the center of the dent which lies on the mid-circumference of the shell; $w(\theta, z)$ is the residual normal displacement caused by the indentation.

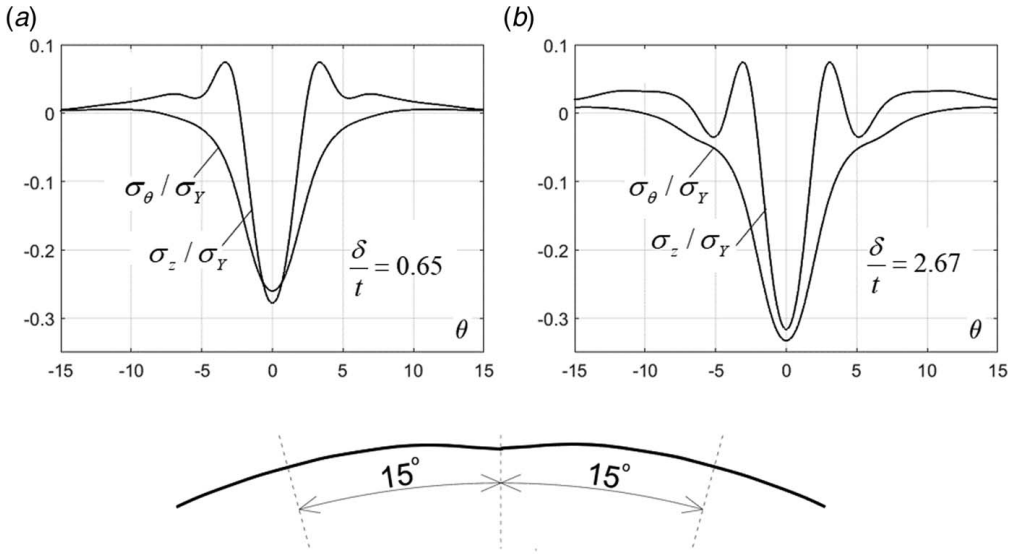

Fig. 8 In-plane stresses averaged through the thickness and normalized by the yield stress plotted along the circumferential arc passing through the center of the dent of the reference shell, (*a*) for a dent amplitude $\delta/t = 0.65$ and (*b*) for $\delta/t = 2.67$

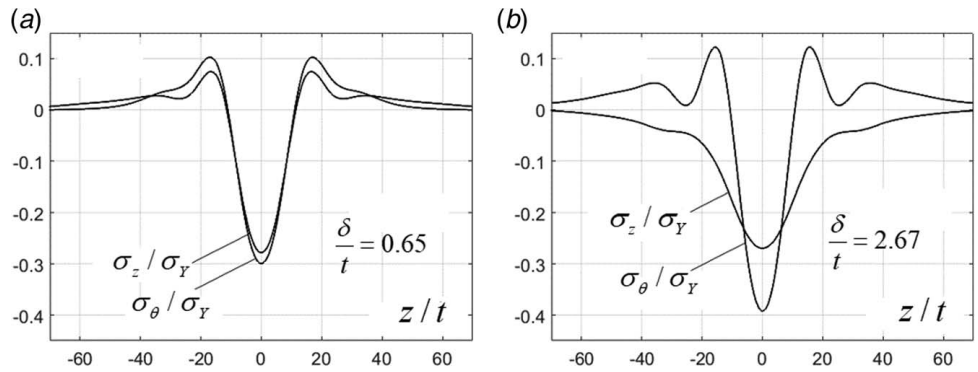

Fig. 9 In-plane stresses averaged through the thickness and normalized by the yield stress plotted along the axial line passing through the center of the dent of the reference shell, (*a*) for a dent amplitude $\delta/t = 0.65$ and (*b*) for $\delta/t = 2.67$

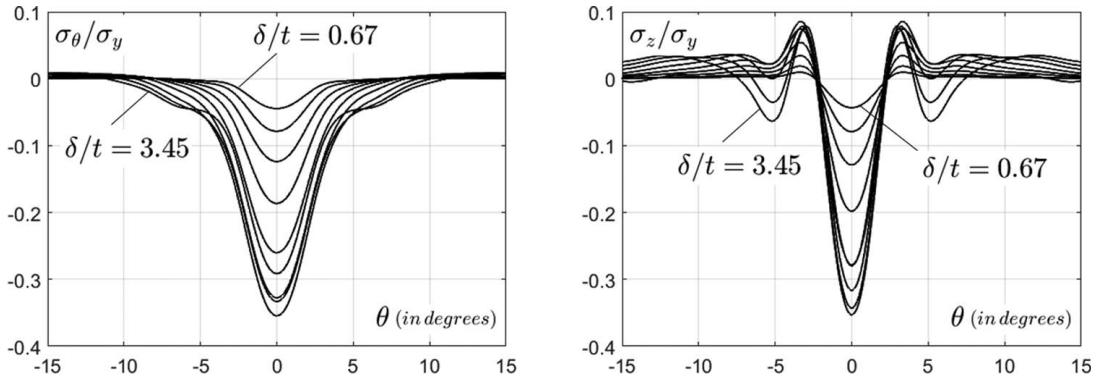

Fig. 10 In-plane stresses averaged through the thickness and normalized by the yield stress plotted along the circumferential arc passing through the center of the dent of the reference shell, with increasing dent amplitude

loading, as seen in Fig. 6, and upon unloading, contact between indenter and shell is lost at point D. The resultant dent amplitude is approximately $\delta/t = 3.4$ in this example.

The results for the residual dent amplitude (the maximum inward residual normal displacement) in Fig. 6 reveal that there is essentially no sensitivity to the indenter radius over the range of radii and depth of indentation considered in the present study. In addition, the results show that for maximum indenter displacements below about $\Delta/t \cong 20$ (or about 10 times the thickness after first contact), essentially no plasticity occurs during indentation, and there is no residual dent. The contrast with the spherical shell is striking. In Fig. 2, it is seen that plasticity sets in at indent displacements of about ½ a thickness and substantial residual dents in the sphere, i.e., $\delta/t > 1$, are produced by indentation amplitudes of only 3–5 times the shell thickness. Comparable dents in the cylindrical shell require indentation amplitudes of more than 20 times the shell thickness after first contact. The non-zero Gaussian curvature of the sphere creates a much stronger coupling between bending and stretching than is the case for the cylinder which has zero Gaussian curvature. Further ramifications of this difference are evident in the shape of the residual dent in Fig. 7 discussed next.

The two plots in Fig. 7 show the residual normal displacement following the indentation of the shell for the example in Fig. 5. Figure 7(*a*) shows the residual displacement around the circumference emanating from the center of the dent (at the middle of the shell) with the center taken to be at $\theta = 0$. Figure 7(*b*) displays the residual displacement along the axial direction (the z-direction) with the center taken to be at $z = 0$. In the circumferential direction, the shape and extent of the dent is similar to that of the spherical shell in Fig. 1. For a cylindrical shell with $R/t = 286$, the dent half-width of about $\theta = 10$ deg corresponds to a circumferential distance of 50 t. By contrast, the effective half-length of the dent in the axial direction is not well defined, and it decays gradually toward the ends of the shell at $z = \pm 520t$. The significant spread of the residual deflection in the axial direction also reflects the fact that the cylindrical shell has zero Gaussian curvature.

Residual stresses in the reference shell are plotted in Figs. 8 and 9 for two levels of dent amplitude, $\delta/t = 0.65$ and 2.67. Figure 8 displays the circumferential and axial in-plane stresses, $\sigma_\theta(\theta, 0)$ and $\sigma_z(\theta, 0)$, along the mid-circumference of the shell, averaged through the thickness and normalized by the initial yield stress. Figure 9 displays the same stresses averaged and normalized similarly but along the axial line passing through the center of the dent, i.e., $\sigma_\theta(0, z)$ and $\sigma_z(0, z)$. The residual average in-plane stresses are dominantly compressive and have a value of about $-0.3\ \sigma_Y$ at the center of the dent for both dent amplitudes. The residual in-plane stresses are also localized in the vicinity of the dent, comparable to the behavior of the dented spherical shell. Unlike the cylindrical shell's residual normal deflection, the residual stresses do not extend farther in the axial direction than in the circumferential direction.

The variation of residual stresses with increasing residual dent amplitude are plotted in Figs. 10 and 11. Figure 10 presents the circumferential and axial in-plane stresses $\sigma_\theta(\theta, 0)$ and $\sigma_z(\theta, 0)$, along the mid-circumference of the shell, averaged through the thickness and normalized by the initial yield stress. Figure 11 presents the same stresses averaged and normalized similarly but along the axial line passing through the center of the dent, i.e., $\sigma_\theta(0, z)$ and $\sigma_z(0, z)$. For smaller dent amplitudes, the residual stresses tend to be smaller as expected.

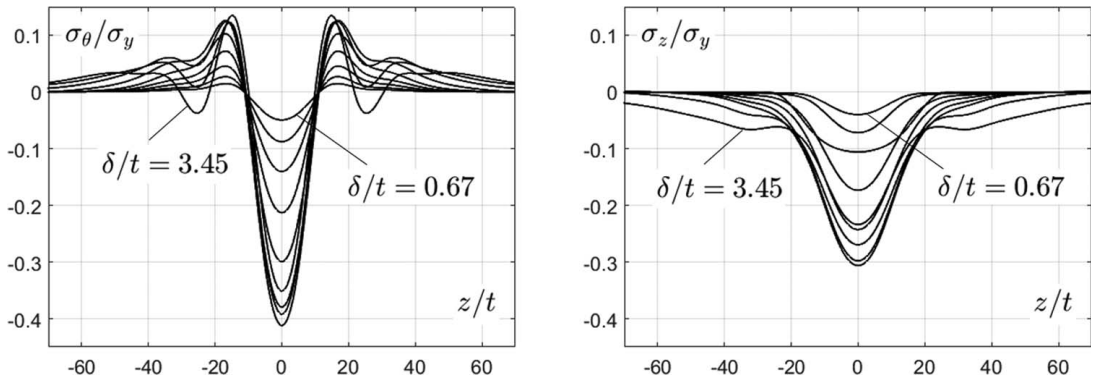

Fig. 11 In-plane stresses averaged through the thickness and normalized by the yield stress plotted along the axial line passing through the center of the dent of the reference shell, with increasing dent amplitude

5 Cylindrical Shells: Step 2, Buckling of the Dented Shell Under Axial Compression—Four Analyses

Four distinct analyses of the dented reference cylindrical shell have been performed: two elastic buckling analyses, one ignoring the residual stress and the other accounting for the residual stresses; and two elastic–plastic buckling analyses, one ignoring the residual stress and the other accounting for the residual stresses. The geometry of the dent is accounted for in all four analyses. As noted earlier, the shells are fully clamped at the ends suppressing end rotation, and the axial displacement Δ of one end toward the other is imposed. The axial displacement is increased until a first maximum in the axial compressive force, F_{max}, is attained which is defined as the buckling load. In some cases, this first maximum is followed by a drop in axial force which is in turn followed by a subsequent increase in axial force. For most of the range of parameters for the examples analyzed here, the buckling loads plotted correspond to global buckling in the sense that the load is a maximum. In some cases, however, the buckling load corresponds to a local maximum such that the shell can support somewhat larger loads beyond this point. In these cases, the deflections associated with the local buckling are relatively large so that, even though local, the buckling is likely to be regarded as undesirable from a structural standpoint. We consider the first local maximum as the buckling load because significant deflections occur at this stage in the loading history [13]. The results of the four analyses are presented in Fig. 12 as F_{max}/F_C versus the dent amplitude δ/t.

Recall that the reference shell (a typical soda can) has been designed to buckle elastically with $\sigma_Y/\sigma_C = 1.95$. Figure 12 reveals that, indeed, plasticity plays no role in the buckling of the shell as can be inferred from the fact that the predictions of the full elastic–plastic buckling analysis and the elastic buckling analysis are essentially identical whether residual stresses are included or not. This is completely consistent with our findings for the spherical shell. The role of the dent's residual stress is also consistent with what was found for the spherical shell. An analysis which accounts for the residual stress of the dent predicts buckling loads that are between 15 and 30% lower than those predicted accounting only for the dent geometry for almost all dent amplitudes except the smallest. To summarize, the main message of this paper conveyed clearly by Fig. 12 is that even if the shell buckles elastically, the effect of the residual stresses associated with the imperfections should not be ignored in a buckling analysis aimed at assessing imperfection-sensitivity.

The role of the shell yield stress is presented in Fig. 13. The perfect shell prior to denting has the same geometry as the reference shell. Only the yield stress is varied in this figure. For each value of

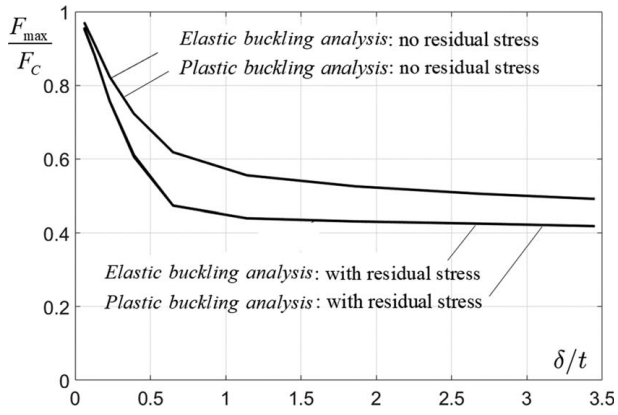

Fig. 12 Axial buckling load of the dented reference shell normalized by the classical elastic buckling load as a function of the dent amplitude δ/t. The results of four distinct buckling analyses are presented: an elastic buckling analysis with and without the residual stresses and a full elastic–plastic analysis with and without the residual stresses.

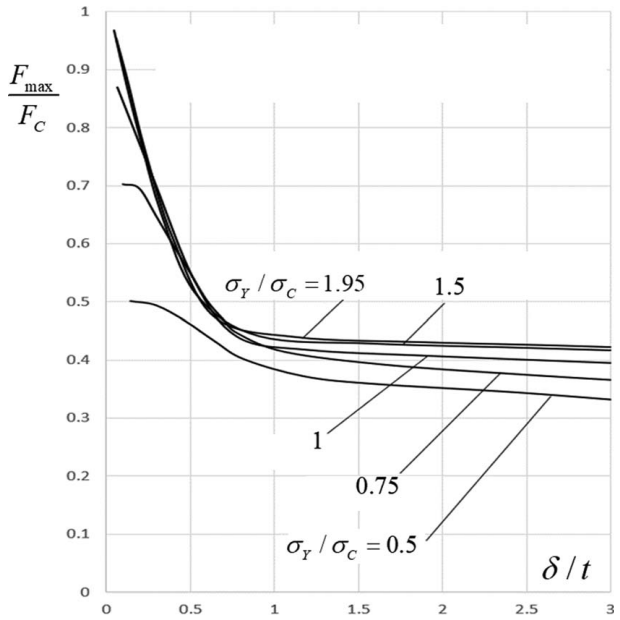

Fig. 13 Axial buckling load of dented cylindrical shells normalized by the classical elastic buckling load as a function of the dent amplitude δ/t for various ratios of yield stress to classical buckling stress. Each of the buckling analyses in Step 2 is a full elastic–plastic analysis accounting for both the geometry of the dent and the residual stress. Dents are created for each of the respective values of σ_Y/σ_C and for each dent amplitude. Prior to denting, all the shells are perfect having the same geometry as the reference shell. The curve for the reference shell is the upper curve labeled by $\sigma_Y/\sigma_C = 1.95$.

the yield stress in Fig. 13, the shell is dented to produce a given dent amplitude (Step 1) and then followed as a continuing calculation (in Step 2) by an elastic–plastic buckling analysis accounting for both the geometry and residual stress of the dent. The trends in Fig. 13 as dependent on σ_Y/σ_C are similar to those discussed for the spherical shell in Fig. 4. Specifically, except for the smallest imperfection amplitudes, plasticity in Step 2 has only a minor effect on the buckling load if $\sigma_Y/\sigma_C \geq 1$. Only for lower values of the yield stress, i.e., $\sigma_Y/\sigma_C < 1$, does plasticity have an appreciable effect on the predictions of the buckling load. Like the results for the spherical shell under external pressure, the results for the cylindrical shell under axial compression confirm the assertion that a highly imperfection-sensitive shell designed to buckle elastically when perfect, i.e., $\sigma_Y/\sigma_C \geq 1$, will indeed buckle elastically—or nearly so—even if imperfect. This assertion is also in accord with an early result [20] for buckling of axially compressed cylindrical shells with sinusoidal geometric axisymmetric imperfections: If $\sigma_Y/\sigma_C \geq 1.05$, no plastic yield occurs before the buckling load is attained for any imperfection amplitude, while if $\sigma_Y/\sigma_C = 1$, plastic yielding occurs only for very small imperfection amplitudes.

6 Concluding Remarks

Localized dent imperfections have been created in otherwise perfect spherical and cylindrical shells by indenting them into the plastic range. The primary focus is on shells that are designed to buckle elastically such that $\sigma_Y/\sigma_C \geq 1$ where σ_C is the compressive buckling stress of the perfect shell. The geometry and the residual stress associated with the dent imperfection are computed. The dented shells are then analyzed for buckling, under external pressure for the spherical shell and under axial compression for the cylindrical shell. Both elastic and elastic–plastic buckling analyses have been performed and, with the aim of assessing how important the residual stress are, separate analyses were carried out: one ignoring the residual stresses and the other taking them into account.

On the one hand, the findings confirm the long-held view that the geometry of the imperfection (the deflection of the mid-surface from the perfect shape) is the most important consideration in analyzing buckling imperfection-sensitivity of unstiffened shells. On the other hand, the results of this paper reveal that, for dimple-like imperfections created by denting, the residual stress can reduce the buckling load by an additional 15–30% below what is predicted based on an analysis only accounting for the imperfection geometry. For shells that are designed to buckle elastically, this is not due to plasticity occurring in the buckling process, rather it is the boost in local compression in the shell in the region of the dent that enhances the susceptibility to buckling. The implication for shell designers who wish to bypass the most conservative shell buckling criteria by relying on the measurement of shell imperfections and incorporating them into their buckling analyses is that residual stresses will also need to be taken into account, at least for the types of dent imperfections considered here.

It is also worth repeating our finding that, for the two highly imperfection-sensitive shell/loading combinations considered in this paper, the buckling process (as opposed to the denting process) is nominally elastic as long as the yield stress exceeds the elastic buckling stress of the perfect shell, $\sigma_Y/\sigma_C \geq 1$. Plasticity will likely occur beyond the maximum load after buckling is initiated, but little or no plastic yield occurs before the maximum load is attained. As remarked earlier, it is not clear that this rule will hold for shell structures that are less imperfection-sensitive than the sphere under external pressure and the cylinder under axial compression. The dramatic drop of the maximum load with increasing imperfection amplitude for these two shell/loading combinations reduces the stresses that produce plastic yielding. When the drop is less precipitous, stresses may reach yield before the maximum load is attained in an imperfect shell. A systematic study of an example such as the cylindrical shell under external pressure which is inherently less imperfection-sensitive would be enlightening in this regard but, to our knowledge, no such study exists in the literature.

Conflict of Interest

There are no conflicts of interest.

Data Availability Statement

The datasets generated and supporting the findings of this article are obtainable from the corresponding author upon reasonable request. The authors attest that all data for this study are included in the paper.

References

[1] Hilburger, M., 2012, "Developing the Next Generation Shell Buckling Design Factors and Technologies," 53rd AIAA/ASME/ASCE/AHS/ASC Structures, Structural Dynamics and Materials Conference, Structures, Structural Dynamics, and Materials and Co-Located Conferences, Honolulu, HI, Apr. 23–26.

[2] Rotter, J. M., 2017, "Challenges and Their Resolution in Both Philosophy and Process to Exploit Advanced Computation in Shell Structure Design," Proceedings of the SSTA 2017, 11th International Conference on Shell Structures Theory and Applications, Gdansk, Poland, Oct., pp. 2–15.

[3] von Kármán, T., and Tsien, H. S., 1939, "The Buckling of Spherical Shells by External Pressure," J. Aeronaut. Sci., **7**(2), pp. 43–50.

[4] Koiter, W. T., 1945, "On the Stability of Elastic Equilibrium," Dissertation, Delft, Holland, An English translation is available: *Tech. Trans. F* 10, 833.

[5] Peterson, J. P., Seide, P., and Weingarten, V. I., 1965, *Buckling of Thin-Walled Circular Cylinders*, SP-8007, NASA.

[6] Weingarten, W. I., and Seide, P., 1969, *Buckling of Thin-Walled Doubly Curved Shells*, SP-8032, NASA.

[7] Ravn-Jensen, K., and Tvergaard, V. T., 1990, "Effect of Residual Stresses on Plastic Buckling of Cylindrical Shell Structures," Int. J. Solids Struct., **26**(9–10), pp. 993–1004.

[8] Song, S., and Dong, P., 2016, "A Framework for Estimating Residual Stress Profile in Seam-Welded Pipe and Vessel Components Part I: Weld Region," Int. J. Press. Vessels Pip., **146**, pp. 74–86.

[9] Masubuchi, K., 1980, *Analysis of Welded Structures (Residual Stresses, Distortion, and Their Consequences)*, Elsevier, Pergamon, Oxford, pp. 328–335.

[10] Vasilikis, D., Karamanos, S., van Es, S. H. J., and Grensigt, A., 2016, "Ultimate Bending Capacity of Spiral-Welded Steel Tubes—Part II: Predictions," Thin-Walled Struct., **102**, pp. 305–319.

[11] Zheng, J., Liu, Z., and Champliaud, H., 2008, "FEM Dynamic Simulation and Analysis of the Roll-Bending Process for Forming a Conical Tube," J. Mater. Process. Technol., **198**(1–3), pp. 330–343.

[12] Wullschleger, L., 2006, "Numerical Investigation of the Buckling Behaviour of Axially Compressed Circular Cylindrs Having Parametric Initial Dimple Imperfections," Doctoral thesis, ETH, Zurich, Permanent Link.

[13] Gerasimidis, S., Virot, E. E., Hutchinson, J. W., and Rubinstein, S. M., 2018, "On Establishing Buckling Knockdowns for Imperfection-Sensitive Shell Structures," ASME J. Appl. Mech., **85**(9), p. 091010.

[14] Jimenez, F. L., Marthelot, J., Lee, A., Hutchinson, J. W., and Reis, F. M., 2017, "Knockdown Factor for the Buckling of Spherical Shells Containing Large-Amplitude Geometric Defects," ASME J. Appl. Mech., **84**(3), 034501.

[15] Sanders, J. L., 1963, "Nonlinear Shell Theories for Thin Shells," Q. Appl. Math., **21**(1), pp. 21–36.

[16] Koiter, W. T., 1966, "On the Nonlinear Theory of Thin Elastic Shells," Proc. Kon. Ned. Ak. Wet. B, **69**, pp. 1–54.

[17] Hutchinson, J. W., 1972, "On the Postbuckling Behavior of Imperfection-Sensitive Structures in the Plastic Range," ASME J. Appl. Mech., **39**(1), pp. 155–162.

[18] Hutchinson, J. W., and Thompson, J. M. T., 2017, "Nonlinear Buckling Interaction for Spherical Shells Subject to Pressure and Probing Forces," ASME J. Appl. Mech., **84**(6), 061001.

[19] Lykhachova, O., and Evkin, A., 2020, "Effect of Plasticity in the Concept of Local Buckling of Axially Compressed Cylindrical Shells," Thin-Walled Struct., **155**, p. 106965.

[20] Hutchinson, J. W., 1974, "Plastic Buckling," Adv. Appl. Mech., **14**, pp. 67–144.

[21] ABAQUS, 2017, *Software Package, ver. 6.14.4 ed.*, Abaqus/Standard, SIMULIA, Providence, RI.

[22] Yadav, K., Cuccia, N., Virot, E., Rubinstein, S., and Gerasimidis, S., 2020, "A Non-Destructive Technique for the Evaluation of Thin Cylindrical Shells' Axial Buckling Capacity (Under Review).